

# The Structure of Cholesterol in Lipid Rafts

Laura Toppozini,<sup>1</sup> Sebastian Meinhardt,<sup>2</sup> Clare L. Armstrong,<sup>1</sup> Zahra Yamani,<sup>3</sup>  
Norbert Kučerka,<sup>3</sup> Friederike Schmid,<sup>2,\*</sup> and Maikel C. Rheinstädter<sup>1,3,†</sup>

<sup>1</sup>*Department of Physics and Astronomy, McMaster University, Hamilton, Ontario, Canada*

<sup>2</sup>*KOMET 331, Institute of Physics, Johannes Gutenberg-Universität Mainz, Mainz, Germany*

<sup>3</sup>*Canadian Neutron Beam Centre, Chalk River, Ontario, Canada*

(Dated: December 17, 2014)

Rafts, or functional domains, are transient nano- or mesoscopic structures in the plasma membrane and are thought to be essential for many cellular processes such as signal transduction, adhesion, trafficking and lipid/protein sorting. Observations of these membrane heterogeneities have proven challenging, as they are thought to be both small and short-lived. With a combination of coarse-grained molecular dynamics simulations and neutron diffraction using deuterium labeled cholesterol molecules we observe raft-like structures and determine the ordering of the cholesterol molecules in binary cholesterol-containing lipid membranes. From coarse-grained computer simulations, heterogenous membranes structures were observed and characterized as small, ordered domains. Neutron diffraction was used to study the lateral structure of the cholesterol molecules. We find pairs of strongly bound cholesterol molecules in the liquid-disordered phase, in accordance with the umbrella model. Bragg peaks corresponding to ordering of the cholesterol molecules in the raft-like structures were observed and indexed by two different structures: a monoclinic structure of ordered cholesterol pairs of alternating direction in equilibrium with cholesterol plaques, i.e., triclinic cholesterol bilayers.

The liquid-ordered ( $l_o$ ) phase of membranes in the presence of cholesterol was brought to the attention of the life science community in 1997 when Simons and Ikonen [1] proposed the existence of so-called rafts in biological membranes. Rafts were thought to be small, molecularly organized units, providing local structure in fluid biological membranes and hence furnishing platforms for specific biological functions [1–10]. These rafts were supposed to be enriched in cholesterol making them more ordered, thicker and, thus, appropriate anchoring places for certain acylated and hydrophobically-matched integral membrane proteins. The high levels of cholesterol in these rafts led to the proposal that rafts are local manifestations of the  $l_o$  phase, although in most cases the nature of the lipid ordering and the phase state were not established in cells, nor in most model membrane studies [10–12].

Rafts are generally interpreted as some kind of super-particles floating around in an otherwise structureless liquid membrane. However, early work in the physical chemistry of lipid bilayers pointed to the possibility of dynamic heterogeneity [13–16] in thermodynamic one-phase regions of binary systems. The sources of dynamic heterogeneity are cooperative molecular interactions and thermal fluctuations that lead to density and compositional fluctuations in space and time.

A number of ternary phase diagrams have been determined for systems involving cholesterol and two different lipid species. Usually these systems contain a lipid with a high melting point, such as a long-chain saturated phospholipid, and a lipid with a low melting point, such as sphingolipids or unsaturated phospholipids [17], resulting in the observations of micrometer-sized, thermody-

namically stable domains [4, 18–21]. Much less work has been done on cholesterol/lipid binary mixtures, which although seemingly simpler, have proven to be more difficult to study. Evidence for a heterogeneous structure of the  $l_o$  phase, similar to a microemulsion, with ordered lipid nanodomains in equilibrium with a disordered membrane was recently supported both by theory and experiment. The computational work by Meinhardt, Vink and Schmid [22] and Sodt *et al.* [23] and the experimental papers by Armstrong *et al.* [24–26] using neutron diffraction were conducted using binary DPPC/cholesterol and DMPC/cholesterol systems.

We combined coarse-grained molecular dynamics simulations including 20,000 lipid/cholesterol molecules with neutron diffraction using deuterium labelled cholesterol molecules to study the cholesterol structure in the liquid-ordered phase of DPPC bilayers. The simulations present evidence for a heterogenous membrane structure at 17 mol% and 60 mol% cholesterol and the formation of small, transient domains enriched in cholesterol. The molecular structure of the cholesterol molecules within these domains was determined by neutron diffraction at 32.5 mol% cholesterol. Three structures were observed: (1) A fluid-like structure with strongly bound pairs of cholesterol molecules as manifestation of the liquid-disordered ( $l_d$ ) phase; (2) A highly ordered lipid/cholesterol phase where the lipid/cholesterol complexes condense in a monoclinic structure, in accordance with the umbrella model; and (3) triclinic cholesterol plaques, i.e., cholesterol bilayers coexisting with the lamellar lipid membranes.

The simulations use a simple coarse-grained lipid model [27] which reproduces the main phases of DPPC

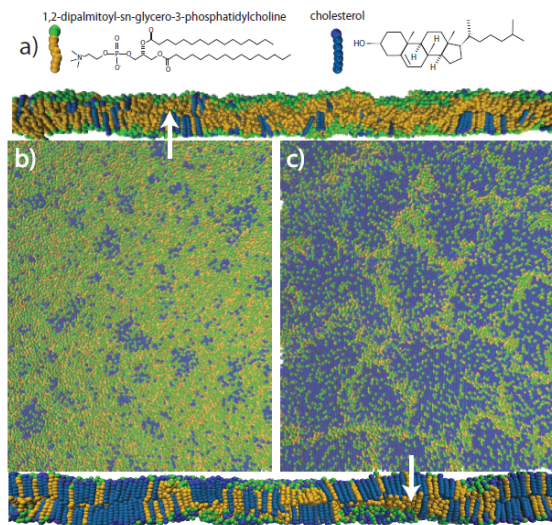


FIG. 1. a) Schematic representation of DPPC and cholesterol molecules used in the simulations. b) Snapshot of the simulation at  $\mu=8.5 k_B T$ , resulting in a cholesterol concentration of  $\approx 17$  mol%. c) Snapshot of the simulation at  $\mu=7.8 k_B T$  resulting in a cholesterol concentration of  $\approx 60$  mol%.

bilayers including the nanostructured ripple phase  $P_{\beta'}$  [27] and has similar elastic properties in the fluid phase [28]. In this model, lipids are represented by short linear chains of beads, with a ‘head bead’ and several ‘tail beads’ (Fig. 1 a)), which are surrounded by a structureless solvent. The model was recently extended to binary lipid/cholesterol mixtures. The cholesterol molecules are modelled shorter and stiffer than DPPC, and they have an affinity to phospholipid molecules, reflecting the observation that sterols in bilayers tend to be solubilized by lipids [29]. In our previous work, we have reported on the behavior of mixed bilayers with small cholesterol content [22]. Locally, phase-separation was observed between a  $l_o$  and a  $l_d$  phase. On large scales, however, the system assumes a two-dimensional microemulsion-type state, where nanometer-sized cholesterol-rich domains are embedded in a  $l_d$  environment. These domains are stabilized by a coupling between monolayer curvature and local ordering [22], suggesting that raft formation is closely related to the formation of ripples in one-component membranes. In the following, we will discuss the behavior of our model membranes at larger cholesterol concentrations and discuss the implications for experiments.

The simulations were done at constant pressure, constant temperature, and constant zero surface tension in a semi-grandcanonical ensemble where lipids and cholesterol molecules can switch their identity. The cholesterol content is thus driven by a chemical potential parameter  $\mu$ . Simulation results are given in units of  $\sigma \approx 6 \text{ \AA}$  [28] and the thermal energy  $k_B T$ . Typical equilibrated sim-

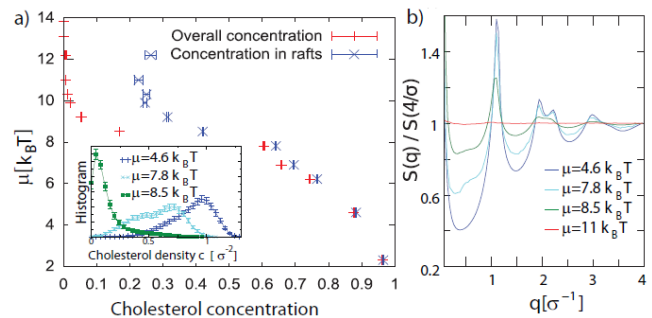


FIG. 2. a) Total cholesterol concentration and cholesterol concentration inside rafts for different chemical potential  $\mu$ . Inset shows a histogram of local cholesterol densities, taken using squares of area  $25\sigma^2 \approx 9 \text{ nm}^2$ . b) Radially averaged two-dimensional lateral structure factor of cholesterol head groups for different  $\mu$  as indicated. The level of molecular order increases with decreasing  $\mu$ , i.e., increasing cholesterol concentration.

ulation snapshots (side view and top view) are shown in Figs. 1 b) and c). At low cholesterol concentration ( $\mu = 8.5 k_B T$ ), one observes small rafts as discussed earlier. At higher cholesterol concentration (lower  $\mu$ ), the cholesterol-rich rafts grow and gradually fill up the system, but they still remain separated by narrow cholesterol-poor ‘trenches’. The side view shows that these trenches have the structure of line defects where opposing monolayers are connected. Such line defects are also structural elements of the ripple phase in one-component bilayers [30, 31].

With increasing cholesterol concentration, the structure of the rafts changes qualitatively. This is demonstrated in Fig. 2 a), which shows that the cholesterol concentration inside rafts remains constant (around 25%) for a range of chemical potentials  $\mu > 8.5 k_B T$ , but then increases rapidly at  $\mu \leq 8 k_B T$ . Along with this concentration increase, the peaks in the lateral structure factor of cholesterol head groups in Fig. 2 b) become more pronounced, indicating a substantial increase in molecular order. We should note that the coarse-grained model used in the simulations is not suitable for studying details of the molecular arrangement inside the ordered structures. However, one can analyze the transition between states with high and low  $\mu$  by analyzing the distribution of local cholesterol densities (Fig. 2 a), inset). At high  $\mu$ , the histogram has a maximum at cholesterol density  $c$  close to zero and decays for higher  $c$  with a broad tail that reflects the contribution of the rafts. At low  $\mu$ , it exhibits a marked maximum at  $c \approx 1\sigma^{-2}$ , corresponding to bilayer regions consisting purely of cholesterol. In the intermediate regime, corresponding to the situation shown in Fig. 1 c), the histogram of cholesterol densities features two broad peaks around  $c \approx 0.4\sigma^{-2}$  and  $c \approx 0.7\sigma^{-2}$ . In this regime, almost pure cholesterol plaques coexist with re-

gions having cholesterol compositions that are close to those of rafts in cholesterol-poor membranes (high  $\mu$  limit in Fig. 2 a)).

The experimental observation of the  $l_o$  phase in a cholesterol lipid binary mixture was initially reported by Vist and Davis [32]. The quantitative determination of binary lipid-cholesterol phase diagrams has remained elusive. In phospholipid membranes, most studies report the  $l_o$  phase at cholesterol concentrations of more than 30 mol% [17]. The formation of cholesterol plaques, phase-separated cholesterol bilayers coexisting with the membrane, was reported to occur at  $\approx 37.5$  mol% cholesterol in model lipid membranes [33]. That leaves a relatively small range of cholesterol concentrations in the experiment (between about 30-37.5 mol%), where the  $l_o$  phase can be studied. Phase-separation may be driven in experiments by certain boundary conditions, not present in computer simulations. The simulations in Fig. 2 can, therefore, access a much larger range of cholesterol concentrations and by studying concentrations slightly lower and higher than the experimentally accessible range, the corresponding structures could be emphasized in the computer model.

We used neutron diffraction to measure the lateral cholesterol structure in DPPC bilayers containing 32.5 mol% at  $T=50^\circ\text{C}$  and a  $\text{D}_2\text{O}$  relative humidity of  $\approx 100\%$ , ensuring full hydration of the membranes. Deuterium labeled cholesterol (d7) was used such that the experiment was sensitive to the arrangements of the cholesterol molecules. Schematics of the two molecules are shown in Fig. 3 a). Highly oriented, solid supported membrane stacks on silicon wafers were prepared, as detailed in the Supplementary Material. The sample was aligned in the neutron beam such that the scattering vector,  $\vec{Q}$ , was placed in the plane of the membranes (Fig. 3 b)). This in-plane component of the scattering vector is referred to as  $q_{\parallel}$ .

Two setups were used: a conventional high energy and momentum resolution setup using a neutron wavelength of  $\lambda=2.37$  Å and a low energy and momentum resolution setup with smaller wavelengths of  $\lambda=1.44$  and 1.48 Å. The latter setup was reported to efficiently integrate over small structures and provide a high spatial resolution capable of detecting small structures and weak signals [12, 25, 35]. The two setups could be readily switched during the experiment by changing the incoming neutron wavelength,  $\lambda$ , without altering the state of the membrane sample. Data taken using the conventional setup are shown in Fig. 3 c) and display a diffraction pattern with broad peaks, typical of a fluid-like structure.

Peaks  $T_1$ ,  $T_2$  and  $T_3$  in Fig. 3 c) correspond to the hexagonal arrangement of the lipid tails with a unit cell of  $a_{\text{lipid-}l_d} = b_{\text{lipid-}l_d} = 5.58$  Å and  $\gamma=120^\circ$ , in agreement with Armstrong *et al.* [25]. By calculating the (coherent) scattering contributions (Table S3), cholesterol and lipid molecules contribute almost equally to the scatter-

|           | Amplitude<br>(counts) | Center<br>(Å <sup>-1</sup> ) | $\sigma_G$<br>(Å <sup>-1</sup> ) | $l_d$ | monoclinic<br>cholesterol<br>$l_o$ -type structure | triclinic<br>cholesterol<br>plaque |
|-----------|-----------------------|------------------------------|----------------------------------|-------|--|------------------------------------|
| Fig. 3 c) | 62                    | 0.75                         | 0.17                             | $H$   |  |                                    |
|           | 117                   | 1.360                        | 0.46                             | $T_1$ |  |                                    |
|           | 27.5                  | 1.360                        | 0.17                             | $C$   |  |                                    |
|           | 46.6                  | 2.289                        | 0.05                             | $T_2$ |  |                                    |
|           | 15.0                  | 2.650                        | 0.10                             | $T_3$ |  |                                    |
| Fig. 3 d) | 19.8                  | 0.5                          | 0.01                             |       |  | [1 0 0]                            |
|           | 34.8                  | 0.55                         | 0.01                             |       | [1 $\bar{1}$ 0]                                    |                                    |
|           | 34.3                  | 0.74                         | 0.01                             |       | [1 0 0]  | [1 1 0]                            |
|           | 33.5                  | 0.98                         | 0.01                             |       |  | [2 0 0]                            |
|           | 110                   | 1.12                         | 0.01                             |       | [2 $\bar{1}$ 0]                                    |                                    |
|           | 117.8                 | 1.32                         | 0.01                             |       | [1 1 0]  |                                    |
|           | 60.0                  | 1.61                         | 0.01                             |       |  | [1 3 0]                            |

TABLE 1. Peak parameters of the correlation peaks observed in Fig. 3 c) and d) and the association with the different cholesterol structures, such as  $l_d$ ,  $l_o$ -type structure and cholesterol plaque.  $H$  and  $C$  label the nearest neighbor distances of lipid head groups and cholesterol molecules, respectively;  $T_1$ ,  $T_2$ , and  $T_3$  denote the unit cell of the lipid tails in the  $l_d$  regions of the membrane. Peaks were fitted using Gaussian peak profiles and widths are listed as Gaussian widths,  $\sigma_G$ .

ing in the  $l_d$  phase such that the corresponding signals are observed simultaneously in Fig. 3 c). Peak  $H$  agrees well with an average nearest neighbor head group-head group distance of  $\approx 8.4$  Å. Peak  $C$  only occurs in the presence of deuterated cholesterol molecules. It was, therefore, assigned to a nearest neighbor distance of  $\approx 4.6$  Å ( $\pm 0.5$  Å) of cholesterol molecules in the  $l_d$  phase, i.e., to pairs of strongly bound cholesterol molecules, as shown in Fig. 3 e). Details of the fitting procedure are given in the Supplementary Material.

Several pronounced Bragg peaks are observed at neutron wavelengths of  $\lambda=1.44$  and 1.48 Å in Fig. 3 d) in addition to the broad correlation peaks. Due to the high cholesterol concentration in  $l_o$ -type structures and plaques and the scattering lengths of DPPC and  $d$ -cholesterol molecules, the corresponding coherent scattering signal in Fig. 3 d) is dominated by the deuterated cholesterol molecules. As listed in Table 1, the peak pattern is well described by a superposition of two 2-dimensional structures: a monoclinic unit cell with lattice parameters  $a_{\text{chol-}l_o} = b_{\text{chol-}l_o} = 11$  Å and  $\gamma=131^\circ$  and a triclinic unit cell with  $a_{\text{chol-plaque}} = b_{\text{chol-plaque}} = 12.8$  Å and  $\gamma=95^\circ$  (the values for  $\alpha$  and  $\beta$  could not be determined from the measurements but were taken from [33, 36] to be  $\alpha = 91.9^\circ$  and  $\beta = 98.1^\circ$ ).

The lipid structure in the  $l_o$ -type structures in binary DPPC/32.5 mol% cholesterol bilayers was recently reported by Armstrong *et al.* from neutron diffraction using deuterium labelled lipid molecules [25]. The lipid tails were found in an ordered, gel-like phase organized in a monoclinic unit cell with  $a_{\text{lipid-}l_o} = b_{\text{lipid-}l_o} = 5.2$  Å and  $\gamma=130.7^\circ$ , as shown in Fig. 3 f). The cholesterol unit cell determined from the diffraction data in Fig. 3 c) is indicative of a doubling of the lipid tail unit cell for the cholesterol molecules. The corresponding cholesterol

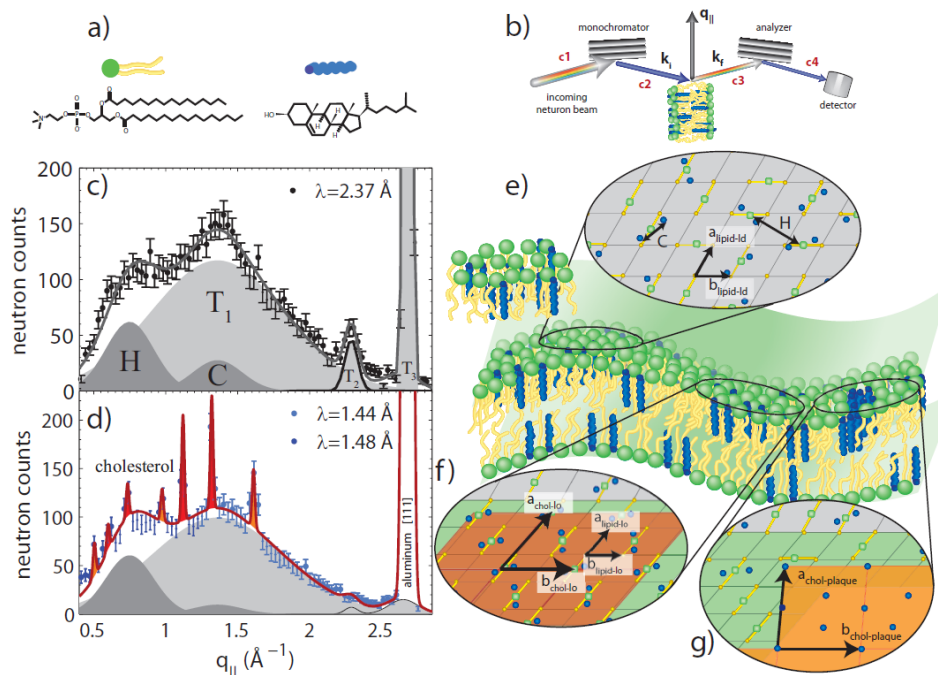


FIG. 3. a) Schematics of DPPC and (deuterated) cholesterol molecules. b) Sketch of the scattering geometry.  $q_{||}$  denotes the in-plane component of the scattering vector. c) Diffraction measured at  $\lambda=2.37$  Å showing broad, fluid-like peaks. d) Data measured at  $\lambda=1.44$  and 1.48 Å. Several pronounced Bragg peaks are observed in addition to the broad peaks in a). e) Cartoon of the different molecular structures: Pairs of cholesterol molecules in the liquid-disordered regions of the membrane in equilibrium with highly ordered cholesterol structures such as the umbrella structure f) and cholesterol plaques g). An aluminum Bragg peak due to the windows of the humidity chamber and the sample holder is present at  $q_{||} = 2.68$  Å<sup>-1</sup>. Aluminum forms a face-centered cubic lattice with lattice parameter  $a=4.04941$  Å [34].

structure consists of cholesterol pairs alternating between two different orientations.

The  $l_d$  and the  $l_o$ -type structures can be related to the well-known umbrella model [37], where one lipid molecule is assumed to be capable to ‘host’ two cholesterol molecules, which leads to a maximum cholesterol solubility of 66 mol% in saturated lipid bilayers. In this scenario the term umbrella model refers to two cholesterol molecules closely interacting with one lipid molecule. Cholesterol plaques, i.e., cholesterol bilayers coexisting with the lamellar membrane phase were reported recently by Barrett *et al.* [33] in model membranes containing high amounts of cholesterol, above 40 mol% for DMPC and 37.5 mol% for DPPC. The triclinic peaks in Fig. 3 d) agree well with the structures published and were, therefore, assigned to cholesterol plaques.

Hence both coarse-grained molecular simulations and neutron diffraction data suggest the coexistence of a liquid disordered membrane with two types of highly ordered cholesterol structures: One with some lipid content (Fig. 3 f), corresponding to the first shoulder in the density histogram at  $\mu = 7.8k_B T$  (Fig. 2 a), inset), and one almost exclusively made of cholesterol (Fig. 3 g), corresponding to the second peak at  $\mu = 7.8k_B T$  in Fig. 2 a). The existence of these structures in the experiment should be robust in binary systems and not depend on, for instance, the sample preparation protocol [38].

The neutron diffraction data present evidence for pairs of strongly bound cholesterol molecules. We note that the scattering experiment was not sensitive to *single* cholesterol molecules, however, the formation of cholesterol dimers with a well defined nearest neighbor distance leads to a corresponding peak in the data in Fig. 3 c) and d).

An attractive force between cholesterol molecules in a POPC bilayer and the formation of cholesterol dimers was reported from MD simulations [39]. Such a force is likely related to the formation of lipid/cholesterol complexes [40] and the umbrella model. However, it is not straightforward to estimate the percentage of dimers from the experiments. A dynamical equilibrium between dimers and monomers is a likely scenario [41].

The dynamic domains observed in this study are not biological rafts, which are thought to be more complex, multi-component structures in biological membranes. In the past, domains have been observed in simple model systems, but only those designed to be ‘raft-forming’ mixtures. In these cases the domains that form are stable equilibrium structures, and are not likely related to the rafts that exist in real cells [12]. The small and fluctuating domains observed in binary systems may be more closely related to what rafts are thought to be [10], and are potentially the nuclei that lead to the formation of rafts in biological membranes. The characteristic overall length scale for nanodomains in the simulations is around  $20\sigma$ , corresponding to 10-20 nanometers. Both simulations and experiments indicate that there are two types of cholesterol-rich patches coexisting with cholesterol-poor liquid-disordered regions, i.e., ordered  $l_o$ -type regions containing lipids and cholesterol and cholesterol plaques. The transition between these two is gradual in the coarse-grained simulations. In real membranes, they have different local structure (monoclinic in  $l_o$ -type regions, triclinic in plaque regions), which may stabilize distinct domains.

This work was supported by the German Science Foundation within the collaborative research center SFB-625.

Simulations were carried out at the John von Neumann Institute for Computing (NIC) Jülich and the Mogon Cluster at Mainz University. Experiments were funded by the Natural Sciences and Engineering Research Council (NSERC) of Canada, the National Research Council (NRC), the Canada Foundation for Innovation (CFI), and the Ontario Ministry of Economic Development and Innovation. L.T. is the recipient of a Canada Graduate Scholarship, M.C.R. is the recipient of an Early Researcher Award from the Province of Ontario.

- 
- [1] K. Simons and E. Ikonen, *Nature* **387**, 569572 (1997)
- [2] K. Simons and E. Ikonen, *Science* **290**, 1721 (2000)
- [3] D. M. Engelman, *Nature* **438**, 578 (2005)
- [4] P. S. Niemelä, S. Ollila, M. T. Hyvönen, M. Karttunen, and I. Vattulainen, *PLoS Comput Biol* **3**, e34 (2007)
- [5] L. J. Pike, *J. Lipid Res.* **50**, S323 (2009)
- [6] D. Lingwood and K. Simons, *Science* **327**, 46 (2010)
- [7] C. Eggeling, C. Ringemann, R. Medda, G. Schwarzmann, K. Sandhoff, S. Polyakova, V. N. Belov, B. Hein, C. von Middendorf, A. Schönle, and S. W. Hell, *Nature* **457**, 1159 (2009)
- [8] F. G. van der Goot and T. Harder, *Seminars in Immunology* **13**, 89 (2001), ISSN 1044-5323
- [9] P.-F. Lenne and A. Nicolas, *Soft Matter* **5**, 2841 (2009)
- [10] K. Simons and M. J. Gerl, *Nat Rev Mol Cell Biol* **11**, 688 (2010)
- [11] O. G. Mouritsen, *Biochim. Biophys. Acta* **1798**, 1286 (2010)
- [12] M. C. Rheinstädter and O. G. Mouritsen, *Curr. Opin. Colloid Interface Sci.* **18**, 440 (2013)
- [13] A. Dibble, A. K. Hinderliter, J. J. Sando, and R. L. Biltonen, *Biophysical journal* **71**, 1877 (1996)
- [14] O. G. Mouritsen and R. L. Biltonen, *New Comprehensive Biochemistry* **25**, 1 (1993)
- [15] O. G. Mouritsen and K. Jørgensen, *Chemistry and physics of lipids* **73**, 3 (1994)
- [16] O. G. Mouritsen and K. Jørgensen, *Current opinion in structural biology* **7**, 518 (1997)
- [17] D. Marsh, *Biochimica et Biophysica Acta (BBA) - Biomembranes* **1798**, 688 (2010)
- [18] H. J. Risselada and S. J. Marrink, *Proc. Natl. Acad. Sci. U.S.A.* **105**, 17367 (2008)
- [19] M. L. Berkowitz, *Biochimica et Biophysica Acta (BBA)-Biomembranes* **1788**, 86 (2009)
- [20] W. Bennett and D. P. Tieleman, *Biochimica et Biophysica Acta (BBA)-Biomembranes* **1828**, 1765 (2013)
- [21] F. A. Heberle, R. S. Petruzielo, J. Pan, P. Drazba, N. Kucerka, R. F. Standaert, G. W. Feigenson, and J. Katsaras, *Journal of the American Chemical Society* **135**, 6853 (2013)
- [22] S. Meinhardt, R. L. C. Vink, and F. Schmid, *Proc. Natl. Acad. Sci. U.S.A.* **110**, 4476 (2013)
- [23] A. J. Sodt, M. L. Sandar, K. Gawrisch, R. W. Pastor, and E. Lyman, *Journal of the American Chemical Society* **136**, 725 (2014)
- [24] C. L. Armstrong, M. A. Barrett, A. Hiess, T. Salditt, J. Katsaras, A.-C. Shi, and M. C. Rheinstädter, *Eur. Biophys. J.* **41**, 901 (2012)
- [25] C. L. Armstrong, D. Marquardt, H. Dies, N. Kučerka, Z. Yamani, T. A. Harroun, J. Katsaras, A.-C. Shi, and M. C. Rheinstädter, *PLOS ONE* **8**, e66162 (2013)
- [26] C. L. Armstrong, W. Häußler, T. Seydel, J. Katsaras, and M. C. Rheinstädter, *Soft Matter* **10**, 2600 (2014)
- [27] F. Schmid, D. Düchs, O. Lenz, and B. West, *Comp. Phys. Comm.* **177**, 168 (2007)
- [28] B. West, F. L. H. Brown, and F. Schmid, *Biophys. J.* **96**, 101 (2009)
- [29] G. Lindblom and G. Orädd, *Biochim. Biophys. Acta* **1788**, 234 (2009)
- [30] A. H. de Vries, S. Yefimov, A. E. Mark, and S. J. Marrink, *Proc. Natl. Acad. Sci.* **102**, 5392 (2005)
- [31] O. Lenz and F. Schmid, *Phys. Rev. Lett.* **98**, 058104 (2007)
- [32] R. Vist and J. H. Davis, *Biochemistry* **29**, 451 (1990)
- [33] M. Barrett, S. Zheng, L. Topozzini, R. Alsop, H. Dies, A. Wang, N. Jago, M. Moore, and M. Rheinstädter, *Soft Matter* **9**, 9342 (2013)
- [34] W. Witt, *Zeitschrift f. Naturforschung* **22a**, 92 (1967)
- [35] C. L. Armstrong, M. A. Barrett, L. Topozzini, N. Kučerka, Z. Yamani, J. Katsaras, G. Fragneto, and M. C. Rheinstädter, *Soft Matter* **8**, 4687 (2012)
- [36] H. Rapaport, I. Kuzmenko, S. Lafont, K. Kjaer, P. B. Howes, J. Als-Nielsen, M. Lahav, and L. Leiserowitz, *Biophysical Journal* **81**, 2729 (2001)
- [37] J. Huang and G. W. Feigenson, *Biophysical Journal* **76**, 2142 (1999)
- [38] E. Elizondo, J. Larsen, N. S. Hatzakis, I. Cabrera, T. Børnholm, J. Veciana, D. Stamou, and N. Ventosa, *Journal of the American Chemical Society* **134**, 1918 (2012)
- [39] Y. Andoh, K. Oono, S. Okazaki, and I. Hatta, *J. Chem. Phys.* **136**, 155104 (2012)
- [40] H. M. McConnell and A. Radhakrishnan, *Biochimica et Biophysica Acta (BBA) - Biomembranes* **1610**, 159 (2003), cholesterol-Rich Domains
- [41] J. Dai, M. Alwarawrah, and J. Huang, *The Journal of Physical Chemistry B* **114**, 840 (2010)
- [42] O. Lenz and F. Schmid, *Journal of molecular liquids* **117**, 147 (2005)
- [43] W. D. Ness, *Chemical Reviews* **111**, 6423 (2011)
- [44] L. Hosta-Rigau, Y. Zhang, M. T. Boon, A. Postma, and B. Städler, *Nanoscale* **5**, 89 (2013)
- [45] D. Schmid, F. and Düchs and B. West, *Comput Phys Commun* **1177**, 168 (2007)
- [46] D. Frenkel and B. Smit, *Understanding molecular simulation: from algorithms to applications* (Academic, 2001)
- [47] N. Chu, N. Kučerka, Y. Liu, S. Tristram-Nagle, and J. F. Nagle, *Phys. Rev. E* **71**, 041904 (2005)
- [48] S. Mabrey and J. Sturtevant, *Proc. Natl. Acad. Sci. USA* **73**, 3862 (1976)
- [49] J. Katsaras, R. F. Epand, and R. M. Epand, *Phys. Rev. E* **55**, 3751 (1997)
- [50] A. Zheludev, "Reslib," <http://www.neutron.ethz.ch/research/resources/reslib> (2009)
- [51] H. Rauch, *Foundation of Physics* **23**, 7 (1993)
- [52] J. R. Taylor, *An Introduction to Error Analysis: The Study of Uncertainties in Physical Measurements* (University Science Books, Sausalito, 1982)

# SUPPLEMENTARY MATERIAL TO: THE STRUCTURE OF CHOLESTEROL IN LIPID RAFTS

## MATERIALS AND METHODS

### *Coarse-Grained Simulation Model*

The model is defined in terms of the length unit  $\sigma \approx 0.6$  nm and the energy unit  $\epsilon \approx 0.36 \cdot 10^{-20}$  J [28]. Phospholipid molecules ( $P$ ) are represented by simple flexible chains of beads with a hydrophilic head and a hydrophobic tail, which self-assemble in the presence of structureless solvent beads [42]. Cholesterol molecules ( $C$ ) have the same basic structure, but they are shorter and stiffer except for one flexible end. All lipids are linear chains of six tail beads attached to one head bead, connected by finite extension nonlinear elastic (FENE) springs with the spring constant  $k_b = 100 \frac{\epsilon}{\sigma^2}$ , equilibrium bond lengths  $r_0 = 0.7\sigma$  ( $P$  lipid) and  $r = 0.6\sigma$  ( $C$  lipid), and logarithmic cutoffs at  $\Delta r_{\max} = 0.2\sigma$  ( $P$ ) and  $\Delta r_{\max} = 0.15\sigma$  ( $C$ ). We have established in previous work that membranes containing pure  $P$  lipids roughly reproduce the behavior of DPPC bilayers [28, 31]. Fully stretched  $C$ -lipid chains have a length of  $3.6\sigma$ , corresponding to  $\sim 22$  Å, which is reasonably close to the estimated length  $\sim 19$  Å of cholesterol molecules [43, 44]. Consecutive bonds in a chain with angle  $\theta$  are subject to a stiffness potential  $U_{BA}(\theta) = k_\theta(1 - \cos(\theta))$  with stiffness constant  $k_\theta = 4.7\epsilon$  ( $P$  lipids),  $k_\theta = 100\epsilon$  ( $C$  lipids, first four angles), and  $k_\theta = 4.7\epsilon$  ( $C$  lipid, last angle). Beads that are not directly bonded with each other interact via a Lennard-Jones potential  $U_{LJ}(r/\zeta) = \epsilon_{LJ} \left( \left( \frac{\zeta}{r} \right)^{12} - 2 \left( \frac{\zeta}{r} \right)^6 \right)$ , which is truncated at a cutoff radius  $r_c$  and shifted such that it remains continuous. At  $r_c = 1$ , one recovers the purely repulsive Weeks-Chandler-Anderson potential [45]. The interaction parameters for pairs of  $P$  or  $C$  beads (head or tail) and solvent beads are taken from [22] and given in Table S2.

| Bead type-bead type     | $\epsilon/\epsilon$ | $\zeta/\sigma$ | $r_c/\zeta$ |
|-------------------------|---------------------|----------------|-------------|
| Head(any)-head(any)     | 1.0                 | 1.1            | 1.0         |
| Head(any)-tail(any)     | 1.0                 | 1.05           | 1.0         |
| Head(any)-solvent       | 1.0                 | 1.1            | 1.0         |
| Tail( $P$ )-tail( $P$ ) | 1.0                 | 1.0            | 2.0         |
| Tail( $P$ )-tail( $C$ ) | 1.0                 | 1.0            | 2.0         |
| Tail( $C$ )-tail( $C$ ) | 0.9                 | 1.0            | 2.0         |
| Tail(any)-solvent       | 1.0                 | 1.05           | 1.0         |
| Solvent-solvent         | 0                   | 0              | 0           |

TABLE S2. Interaction parameters of the coarse-grained molecular dynamics simulations.

Hence, all non-bonded interactions except the tail-tail interactions are repulsive, and the attraction between  $C$  tail beads is weaker than that between other tail beads, which effectively leads to an enhanced affinity between  $C$ -chains and  $P$ -chains. The model was studied by Monte Carlo simulations at constant pressure  $P = 2\epsilon/\sigma^3$  and constant zero surface tension in a fluctuating box of variable size and shape [45]. The total number of lipids was kept fixed, but the composition was allowed to fluctuate (semi-grand canonical ensemble). This was implemented by means of

configurational bias Monte Carlo moves [46], during which the identity of a lipid was switched between  $P$  and  $C$ . The use of the semi-grand canonical ensemble was necessary to ensure that the configurations could be equilibrated and that the finite domains were not simply the result of an incomplete phase separation. Even in the semi-grand canonical ensemble, the equilibration times were still of order 1-3 million Monte Carlo sweeps. Simulations were carried out at the John von Neumann Institute for Computing (NIC) Jülich and the Mogon Cluster at Mainz University.

### *Sample Preparation and Neutron Diffraction Experiment*

Deuterated cholesterol (d7) was used to enhance the intensity of the out-of-plane and in-plane neutron Bragg diffraction peaks. Highly oriented, multi-lamellar stacks of 1,2-dipalmitoyl-sn-glycero-3-phosphocholine (DPPC) with 32.5 mol% cholesterol-d7 were prepared on 2" single-side polished Si wafers of thickness 300  $\mu\text{m}$ . A solution of 16.7 mg/mL DPPC with 32.5 mol% cholesterol in 1:1 chloroform and 2,2,2-trifluoroethanol (TFE) was prepared. The Si wafers were cleaned by alternate 12 minute sonications in ultra pure water and methanol at 313 K. This process was repeated twice. The cleaned wafers were placed on a heated sample preparation surface, which was kept at 50°C. This temperature is well above the main phase transition for DPPC, thus the heated substrates ensured that the lipids were in the fluid phase after deposition. 1.2 mL of the lipid solution was deposited on each Si wafer and allowed to dry. The wafers were kept under vacuum overnight to remove all traces of the solvent. Samples were then hydrated with heavy water,  $\text{D}_2\text{O}$ , and annealed in an incubator at 328 K for 24 hours. Following this protocol, each wafer contained  $\approx 3,000$  highly oriented stacked membranes with a total thickness of  $\approx 10 \mu\text{m}$ . Sixteen such Si wafers were stacked with two 0.3 mm aluminum spacers placed in between each wafer to allow for the membranes to be properly hydrated. The "sandwich" sample was kept in a sealed temperature and humidity controlled aluminum chamber. Hydration of lipid membranes from water vapor was achieved by independently adjusting the temperature of the heavy water reservoir, the sample and the chamber cover. Temperature sensors were installed close to the sample. A water bath was used to control the temperature of the  $\text{D}_2\text{O}$  reservoir, and the temperatures of the sample and its cover were controlled using Peltier elements.

### *Sample Characterization*

The sample was mounted vertically in the neutron beam such that the scattering vector,  $Q$ , could either be placed in the plane of the membranes ( $q_{\parallel}$ ), or perpendicular to it ( $q_z$ ), as shown in Fig. 3 b). The out-of-plane and in-plane structures could be measured by simply rotating the sample by 90°. The lamellar spacing,  $d_z$ , i.e., the distance between two neighboring membranes in the stack, was determined from neutron diffraction along the membrane normal,  $q_z$ . The corresponding scans are shown in Fig. S1 and show a series of pronounced and equally spaced Bragg peaks indicative of uniform and well developed lamellar membrane stacks. A concentration of 32.5 mol% cholesterol was previously carefully checked by Armstrong *et al.* and confirmed to be in the liquid-ordered state for DPPC membranes [25]. Scans were measured for different neutron wavelengths,  $\lambda$ , and over the duration of the experiment of about 3 weeks. The bilayer spacing stayed within the range of 57.8 Å and 59.2 Å, corresponding to a hydration of the bilayers to better than 99.6% [47]. The main transition temperature,  $T_m$ , of DPPC is reported to be  $T = 314.4 \text{ K}$  [48, 49].

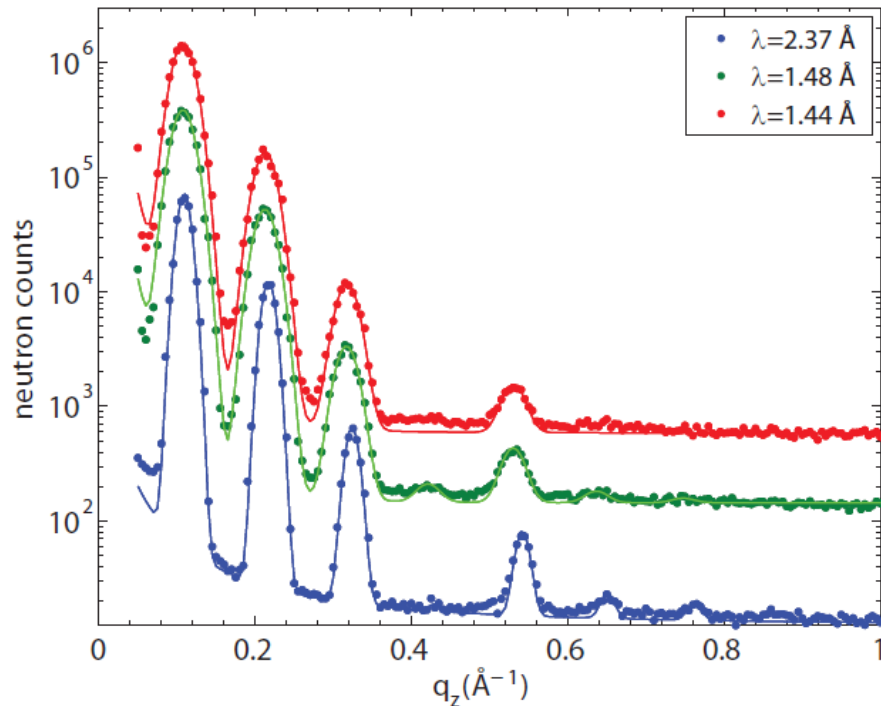


FIG. S1. Neutron diffraction data for each scattering wavelength used to probe the out-of-plane structure along the membrane normal,  $q_z$ . The wavelength  $2.37 \text{ \AA}$  is the wavelength used in conventional neutron scattering setups, while wavelengths  $1.48 \text{ \AA}$  and  $1.44 \text{ \AA}$  were used in for the low energy, low  $Q$  resolution setups.

All measurements reported here were done at  $T = 323.2 \text{ K}$  ( $50^\circ\text{C}$ ), well above  $T_m$ .

#### *Scattering Cross Sections of the Different Molecular Components*

To determine the contribution of lipid and cholesterol molecules to the scattering signals, the corresponding scattering lengths were calculated and are listed in Table S3. Scattering lengths for protonated and deuterated lipid, cholesterol and water molecules are included for completeness. Scattering from lipid molecules dominates the scattering signal in a DPPC-d62/32.5 mol% cholesterol system. Lipid and cholesterol molecules have equal scattering contributions in the liquid-disordered phase at DPPC/66 mol% cholesterol-d7 and both signals were observed in the data in Fig. 3 c). However, cholesterol molecules dominate at higher concentrations of, e.g., DPPC/66 mol% cholesterol-d7 in  $l_o$ -type or plaque structures (as seen in Fig. 3 d)).

|                               | Molecule       | Chemical Formula  | Scattering Length (fm) |
|-------------------------------|----------------|---|------------------------|
|                               | DPPC           | C <sub>40</sub> H <sub>80</sub> NO <sub>8</sub> P                 | 27.63                  |
|                               | DPPC-d62       | C <sub>40</sub> H <sub>18</sub> D <sub>62</sub> NO <sub>8</sub> P | 673.1                  |
|                               | Cholesterol    | C <sub>27</sub> H <sub>46</sub> O                                 | 13.25                  |
|                               | Cholesterol-d7 | C <sub>27</sub> H <sub>39</sub> D <sub>7</sub> O                  | 86.12                  |
|                               | Water          | H <sub>2</sub> O  | -1.68                  |
|                               | Heavy Water    | D <sub>2</sub> O  | 19.15                  |
| DPPC/32.5 mol% Cholesterol-d7 | DPPC           | C <sub>40</sub> H <sub>80</sub> NO <sub>8</sub> P                 | 18.65                  |
|                               | Cholesterol-d7 | C <sub>27</sub> H <sub>39</sub> D <sub>7</sub> O                  | 27.99                  |
| DPPC/66 mol% Cholesterol-d7   | DPPC           | C <sub>40</sub> H <sub>80</sub> NO <sub>8</sub> P                 | 9.11                   |
|                               | Cholesterol-d7 | C <sub>27</sub> H <sub>39</sub> D <sub>7</sub> O                  | 56.84                  |

TABLE S3. Scattering lengths of the different membrane components.

*Neutron Diffraction Experiment*

Experiments were conducted using the N5 triple-axis spectrometer at the Canadian Neutron Beam Centre (Chalk River, ON, Canada). The three axes of the spectrometer refer to the axis of rotation of the monochromator, the sample and the analyzer. The incident and final neutron energies are defined by the Bragg reflections from pyrolytic graphite (PG) crystals. The divergence of the neutron beam was controlled by Soller collimators. A schematic of the instrument's configuration is shown in Fig. 3 b). The instrumental parameters for the two setups used in this experiment are listed in Table S4. Energy and  $Q$ -resolution (given as FWHM) were calculated using the ResLib software package by A. Zheludev [50] adapted to the N5 spectrometer.

| $\lambda$ (Å) | E (meV) | $\Delta E$ (meV) | $\Delta Q$ (Å <sup>-1</sup> ) |
|---------------|---------|------------------|-------------------------------|
| 2.37          | 14.6    | 0.757            | 0.020                         |
| 1.44          | 39.5    | 3.521            | 0.033                         |
| 1.48          | 37.3    | 3.239            | 0.032                         |

TABLE S4. Instrumental parameters of the triple-axis spectrometer.

The  $\Delta E$  and  $\Delta Q$  of a neutron triple-axis spectrometer are determined by: (1) the incident energy of the neutron beam; (2) the divergence of the neutron beam; and (3) the wavelength resolution of the monochromator and analyzer. Collimation was kept constant during the course of the experiment and set to (c1-c2-c3-c4): 30-18-28-60 (in minutes). Small and large  $\Delta E$  setups were achieved by varying the incident energy of the incoming neutrons. The longitudinal coherence length of the neutron beam,  $\xi$ , is defined by  $\xi = \lambda^2/\Delta\lambda$  [51]. For a neutron spectrometer with incident neutron energy  $E$  and instrumental energy resolution  $\Delta E$ ,  $\xi$  can be estimated to be  $\xi \approx 18\sqrt{E}/\Delta E$  [35], where  $E$  and  $\Delta E$  are in meV.

Note that the reason for the typically low monochromaticity of neutron beams is to avoid further compromising the

already low-flux “white” neutron beam, a situation that is very different for synchrotron X-rays. Switching between the high and low energy resolution setups was done by changing instrumental settings of the neutron triple-axis spectrometer, which has an effect on  $\Delta Q$  and  $\Delta E$  of the beam. A smaller neutron wavelength leads to strongly relaxed  $\Delta Q$  and  $\Delta E$ . In addition, the longitudinal coherence length of the neutron beam decreases. The most significant changes between the high and low energy resolution setups are: (1) a more efficient integration over smaller  $q_{||}$  ranges to enhance small signals; and (2) a reduction of the coherently added scattering volume.

*Details of the Fitting of In-Plane Diffraction Data*

| $\lambda$ (Å) | Lorentzian Amplitude (counts) | Lorentzian Width (Å <sup>-1</sup> ) | Constant Offset (counts) |
|---------------|-------------------------------|-------------------------------------|--------------------------|
| 2.37          | 730                           | 0.45                                | 135                      |
| 1.44          | 1060                          | 0.29                                | 170                      |
| 1.48          | 1000                          | 0.29                                | 175                      |

TABLE S5. Parameters of the background used to fit the in-plane diffraction data. The incoherent scattering contribution was accounted for by a Lorentzian peak shape centered at  $q_{||}=0$  Å<sup>-1</sup>.

The in-plane diffraction data in Figure 3 c) and d) were fit by using a series of Gaussian peak shapes to determine the scattering contributions of lipid and cholesterol molecules. The high total scattering of the sample, due to the large percentage of protonated material, resulted in a large constant,  $Q$ -independent background. While small collimation was used, beam size was 2 inches by 2 inches to optimally illuminate the silicon wafers, leading to a significant scattering contribution at small  $Q$ -values, close to the direct beam. The background was accounted for by a Lorentzian peak centered at  $q_{||}=0$  Å<sup>-1</sup> including a constant. Details of the background for the different wavelengths used are given in Table S5. In contrast to coherent scattering, incoherent scattering is isotropic,  $Q$ -independent and well accounted for by a constant background at larger  $Q$ -values of  $Q \gtrsim 0.45$  Å<sup>-1</sup>.

The in-plane diffraction data were tentatively fit with only lipid tail peaks, lipid tail and head group peaks, and lipid tail, head group and cholesterol peaks, as shown in Fig. S2. The corresponding residuals and  $\chi^2$ -values are given in the figure. Based on the comparison, the model suggested in the main paper including contributions from lipid tails, head groups and cholesterol best describes the experimental data, with a significantly smaller  $\chi^2$ -value.

The uncertainty in the determination of the position of the cholesterol peak (the  $C$ -peak in Fig. 3 c) can tentatively be estimated by fixing the position of the cholesterol peak ( $C$ ) and shifting it by  $\pm 10\%$  with respect to the  $C$  peak position in the original fit. All peak amplitudes were allowed to vary, however, all peak locations were fixed except for the lipid tail ( $T_1$ ) peak. The result of this procedure is shown in Fig. S3. In order to estimate the quality of the fitted curve, the mean (see Eq. (1) from [52]) and standard deviation of the residuals (Eq. (2) from [52]) were calculated:

$$\bar{y} = \frac{\sum_{i=1}^n (y_i^{data} - y_i^{fit})}{n} \quad \text{and} \quad (1)$$

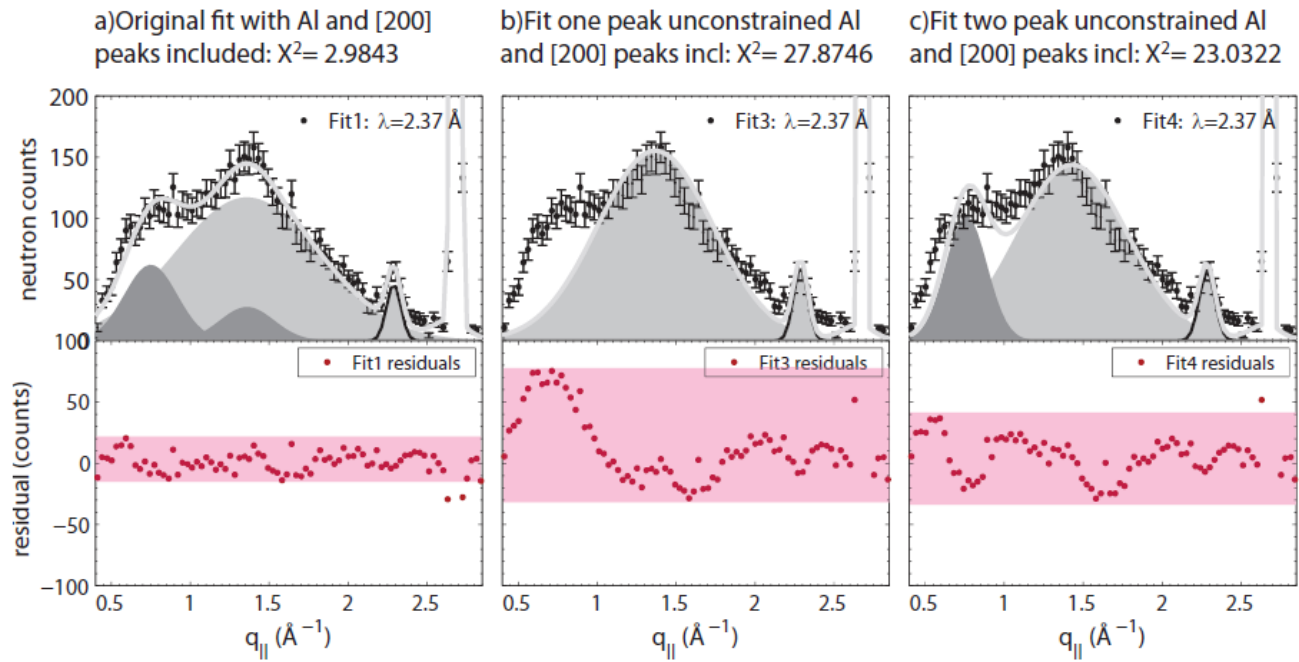


FIG. S2. Comparison of fitting different models to the in-plane diffraction data (Fig. 3 in the main paper). The fit including Gaussians peak profiles from lipid tails and head groups and cholesterol best describes the data with a significantly better  $\chi^2$ -value.

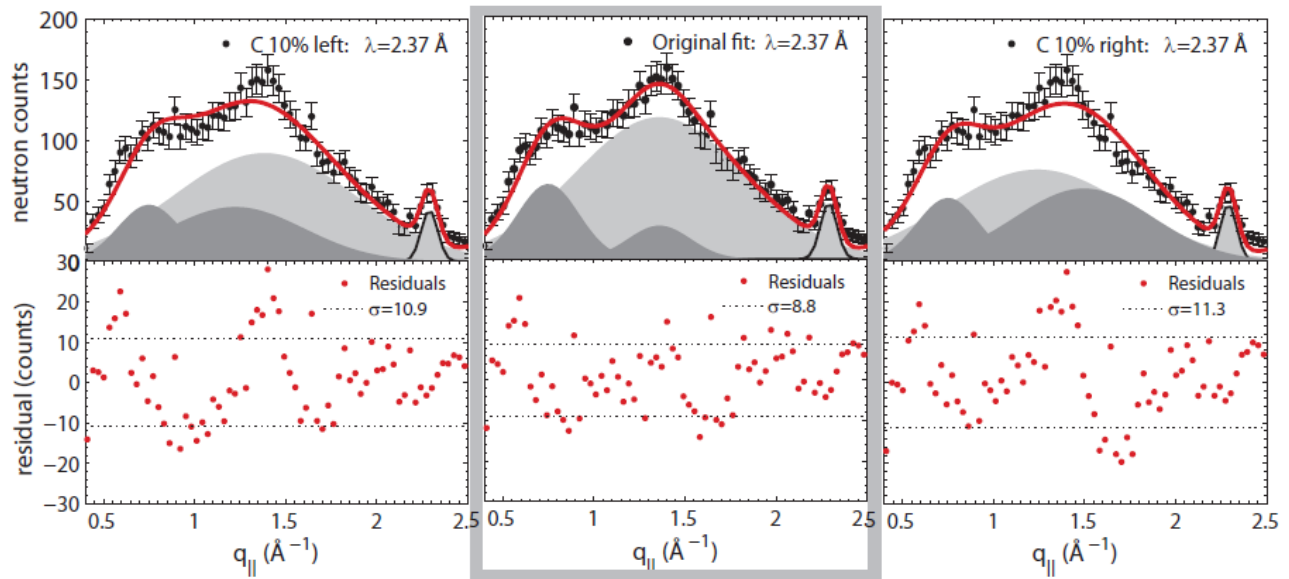


FIG. S3. The uncertainty in determining the position of the cholesterol peak ( $C$ ) can tentatively be estimated by shifting and constraining the peak away from its fitted position and evaluating the quality of the observed fit. The residuals  $((y_i^{data} - y_i^{fit}) - \bar{y})$  are plotted below each fit and the corresponding standard deviations,  $\sigma$ , are listed in the legend.  $\sigma$  was found to increase by  $\approx 25\%$  when the when the  $C$  peak position was changed by more than 10%.

$$\sigma = \sqrt{\frac{\sum_{i=1}^n \left( (y_i^{data} - y_i^{fit}) - \bar{y} \right)^2}{n - 1}}, \quad (2)$$

where  $\bar{y}$  is the mean of the deviation of the data from the fit,  $\sigma$  is the standard deviation from the mean, and  $n$  is the number of data points used in the calculation. The result is shown in Fig. S3. The residuals and standard deviation from (Eq. (2)) are plotted below the fit. Both the fits where the  $C$  peak is fixed to  $q_{||}=1.22 \text{ \AA}$  (equivalent to a shift of 10% to the left) and where the  $C$  peak is fixed to  $q_{||}=1.50 \text{ \AA}$  (equivalent to a 10% to the right) show a significant increase in the standard deviation. We note that the data range used in these calculations does not include the aluminum peak as its high intensity drowns out the quantitative differences in the aforementioned fits.

The analysis can be summarized as follows: the in-plane diffraction data are best described by peaks related to ordering of lipid tails, lipid head groups and cholesterol molecules. Based on the above analysis the uncertainty in the correlation distance between cholesterol molecules in a cholesterol-lipid-cholesterol complex in the liquid disordered phase was tentatively estimated to be 10%, resulting in  $4.6 \pm 0.5 \text{ \AA}$ .